Supporting Information

Atomically dispersed Mn atoms coordinated with N and O within N-doped porous carbon framework for boosted oxygen reduction catalysis

Juanjuan Huo,[a,b] Xianjun Cao,[b] Yaping Tian,[g] Lu Li,[b] Junpeng Qu,[b] Yuhan Xie,[d] Xinming Nie,[*f] Yufei Zhao,[*b] Jinqiang Zhang,[*e] and Hao Liu[*b,c,d]

[a]Institute of Energy Materials Science, University of Shanghai for Science and Technology, Shanghai 200093, China.

[b]Joint International Laboratory on Environmental and Energy Frontier Materials, School of Environmental and Chemical Engineering, Shanghai University, Shanghai 200444, China. Email: Yufei-Zhao@shu.edu.cn

[c]State Key Laboratory of Advanced Special Steel, Shanghai Key Laboratory of Advanced Ferrometallurgy, Shanghai University, Shanghai 200444, China.

[d]Centre for Clean Energy Technology, School of Mathematical and Physical Sciences, Faculty of Science, University of Technology Sydney, Broadway, Sydney, NSW 2007, Australia. Email: Hao.Liu@uts.edu.au

[e]Department of Electrical and Computer Engineering, University of Toronto, 35 St George Street, Toronto, Ontario, M5S 1A4, Canada. Email: jinqiang.zhang@utoronto.ca

[f]School of Physics and Electronic Engineering, Jiangsu Normal University, Xuzhou, Jiangsu 221116, China. Email: nxinming@jsnu.edu.cn

[g]KeWen College, JiangSu Normal University, XuZhou, Jiangsu 221000, China

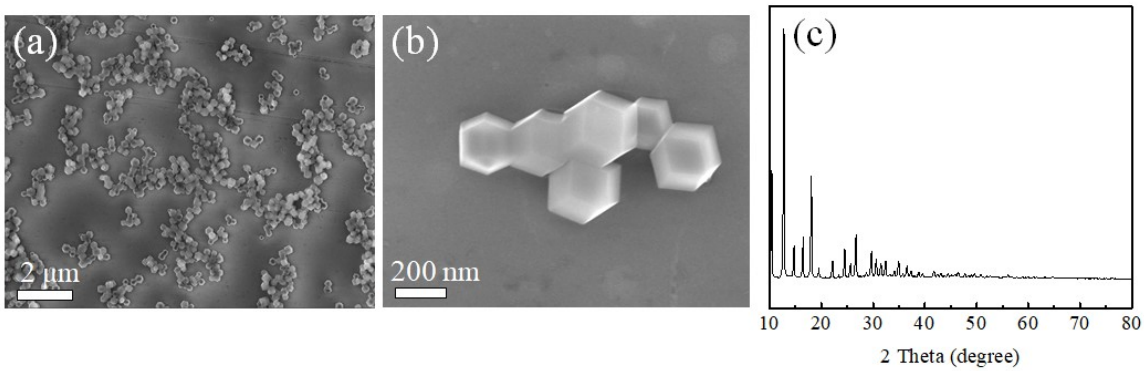

Figure S1. (a and b) SEM images of ZIF-8 sample. (c) Powder XRD pattern of the synthesized ZIF-8 sample.

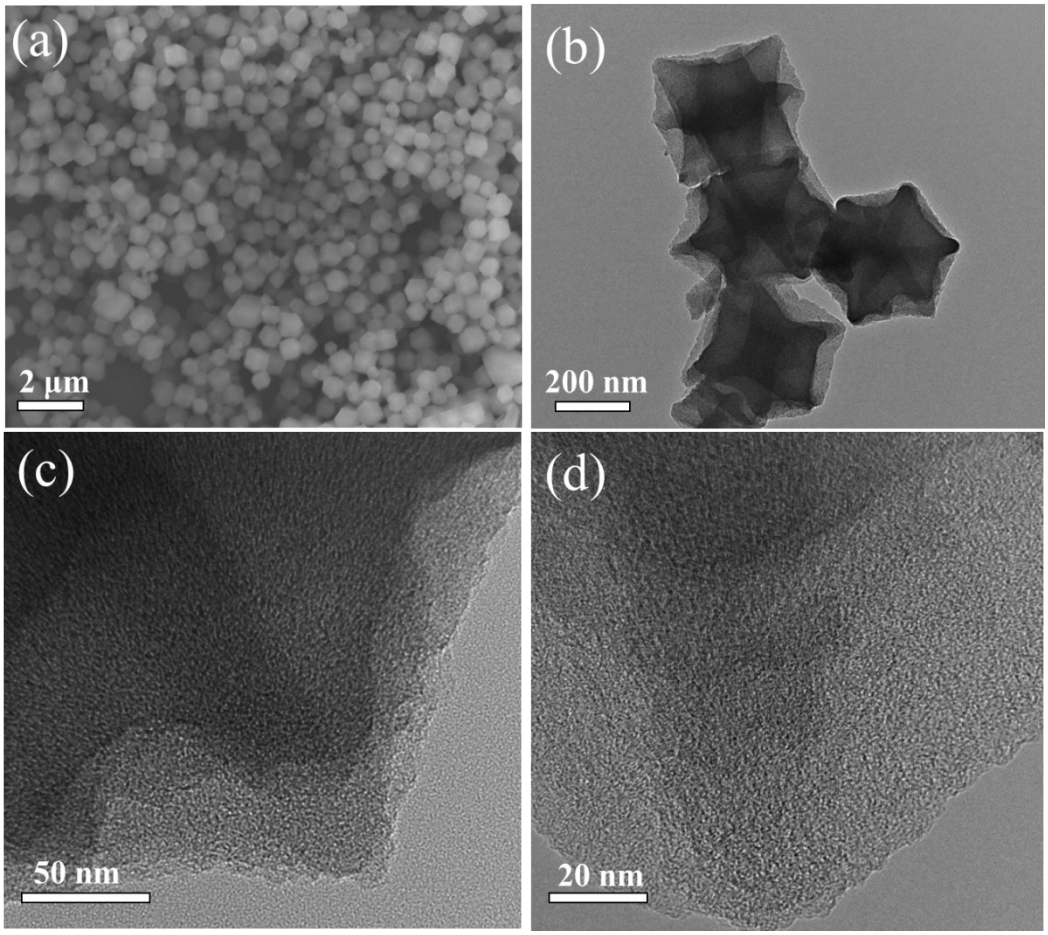

Figure S2. SEM images of the prepared ZIF-8-derived porous carbon (NC) sample.

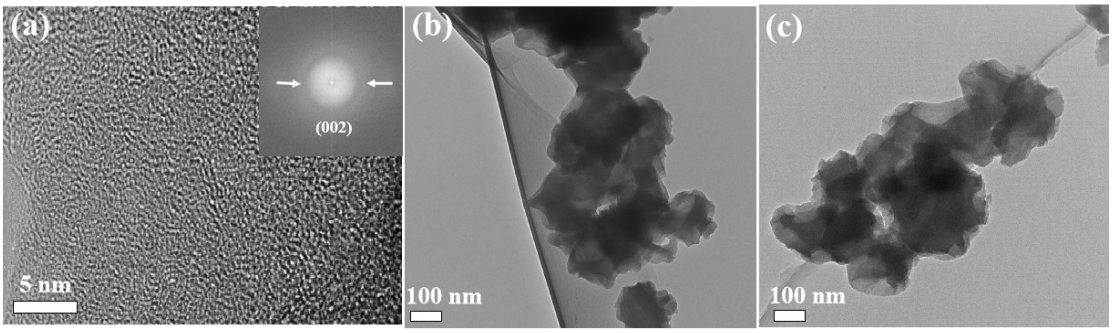

Figure S3. (a) HR-TEM image of Mn-SAs/NC catalyst and corresponding Fast Fourier Transform (FFT) profile. TEM images of (b) Fe-SAs/NC and (c) Cu-SAs/NC samples.

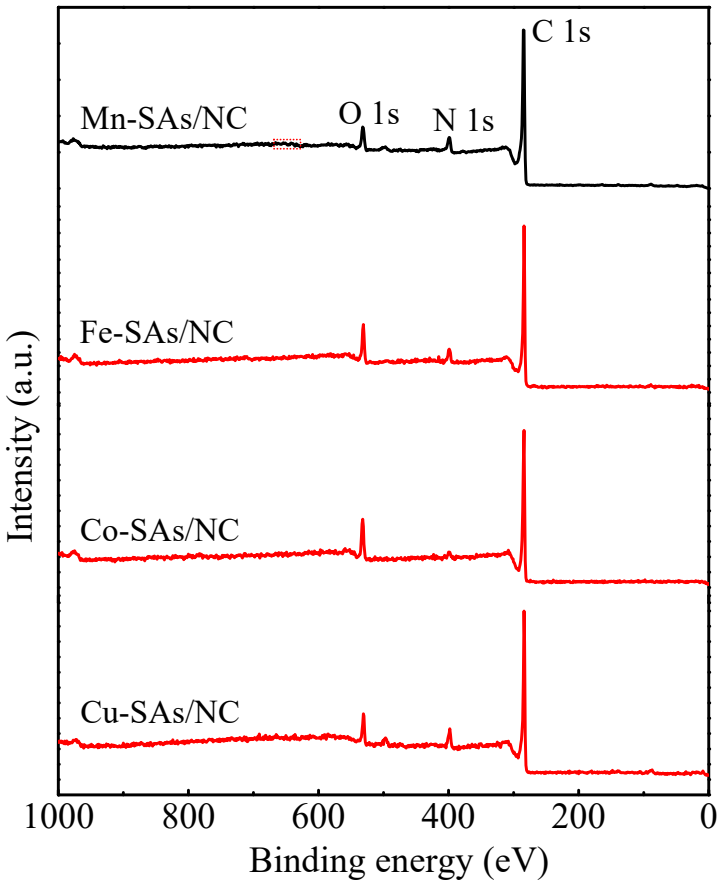

Figure S4. (a) Survey XPS spectra of various samples.

As shown in Fe 2p spectrum, two pairs of peaks at 710.2/723.2 eV and 714.6/726.8 eV are ascribed to Fe^{2+} and Fe^{3+} species, respectively.[1,2] For the Co 2p spectrum, the peaks at binding energies of 780.1 eV and 783.2 eV are characteristic of Co^{2+} and Co^{3+} species, respectively.[3, 4] In the high-resolution Cu 2p spectrum, the divided peaks at 931.1 and 933.7 eV are attributed to the Cu^{+}, and Cu^{2+} species, respectively.[5, 6] No peaks originated from pure metal species can be observed in the various M-SAs/NC, indicating the existence of oxidized metal states.

Table S1. The corresponding atomic contents of as prepared catalysts based on XPS analysis.

Catalysts	C (at.%)	N (at.%)	O (at.%)	metal (at.%)
Mn-SAs/NC	85.15	7.86	6.32	Mn, 0.67
Fe-SAs/NC	82.18	7.16	10.19	Fe, 0.47
Co-SAs/NC	84.17	3.6	11.84	Co, 0.38
Cu-SAs/NC	83.37	8.01	8.38	Cu, 0.24

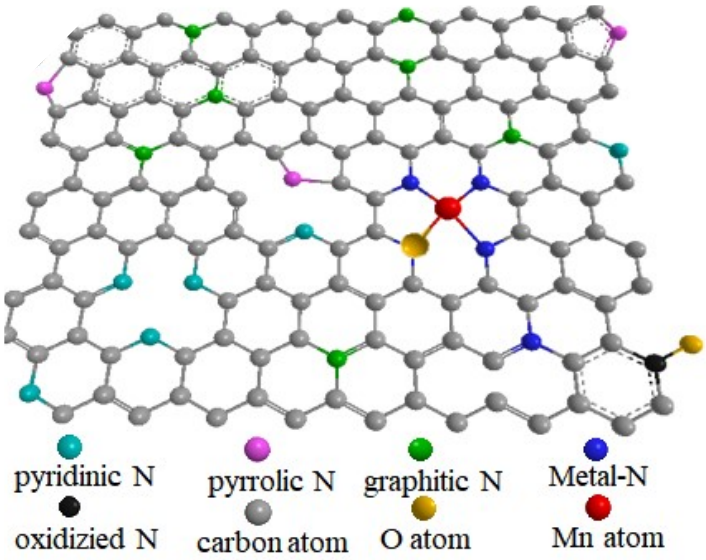

Figure S5. Schematic representation of different types of N atoms within a graphitic layer in Mn-SAs/NC catalyst.

The existed pyridinic-N and graphitic-N benefit to the altering of electronic structures of graphitic carbon, which can effectively facilitate the enhancement of ORR activity.[7, 8] The atomic model of N species on the surface of catalyst was displayed in **Fig. S5**. Typically, the graphitic-N is contributed to the replacement of a carbon atom with a heteroatom N with bonding three sp^2-carbon atoms in the panel of graphene. The pyrrolic-N is a five-round ring consisted of a heteroatom N and four carbon atoms at the edge of graphene. The pyridinic-N locates at the edge of graphene plane with bonding two sp^2-carbon atoms. The oxidized-N reveals that the heteroatom N dopes into carbon matrix with bonding two carbon atoms and oxygen groups.

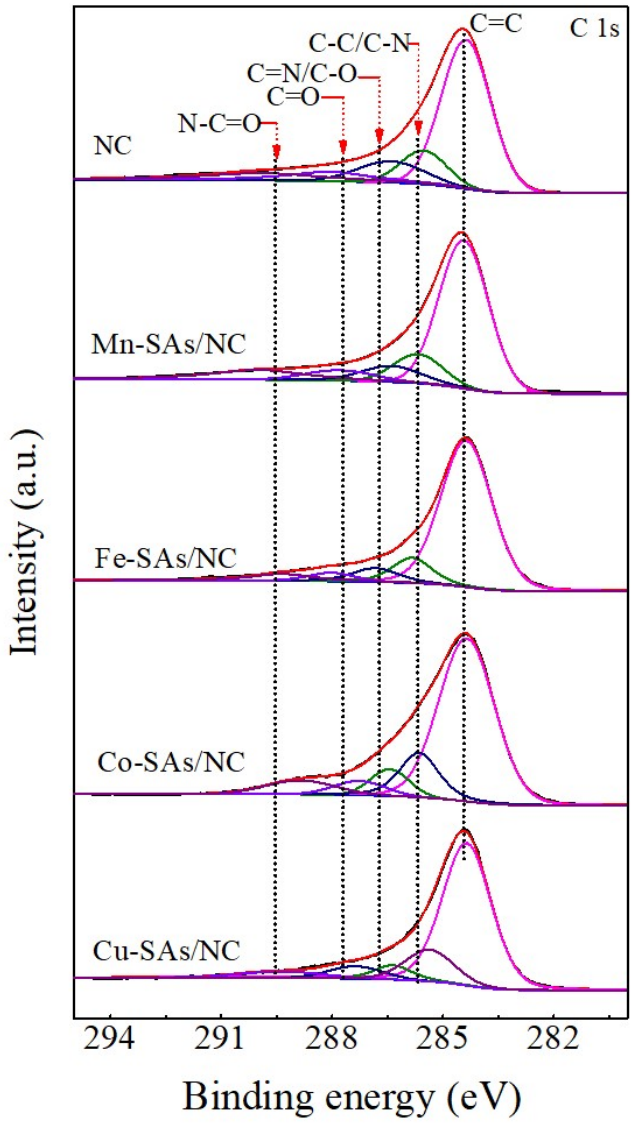

Figure S6. High-resolution C 1s XPS spectra in M-SAs/NC.

For the C 1s XPS spectra in **Fig. S6**, five peaks can be observed at 284.4, 285.3, 286.2, 287.5, and 289.4 eV, corresponding to the C=C, C-C/C-N, C-N/C-O, C=O, and N-C=O, respectively.[9]

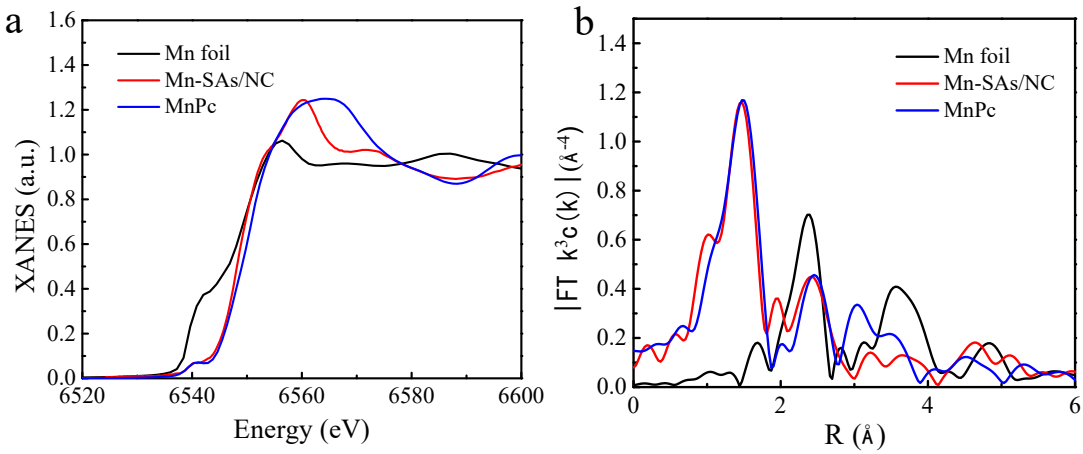

Figure S7. (a) Mn K-edge XANES spectra of Mn foil, MnPc, and Mn-SAs/NC. (b) FT EXAFS spectra at the Mn K-edge of Mn foil, MnPc, and Mn-SAs/NC.

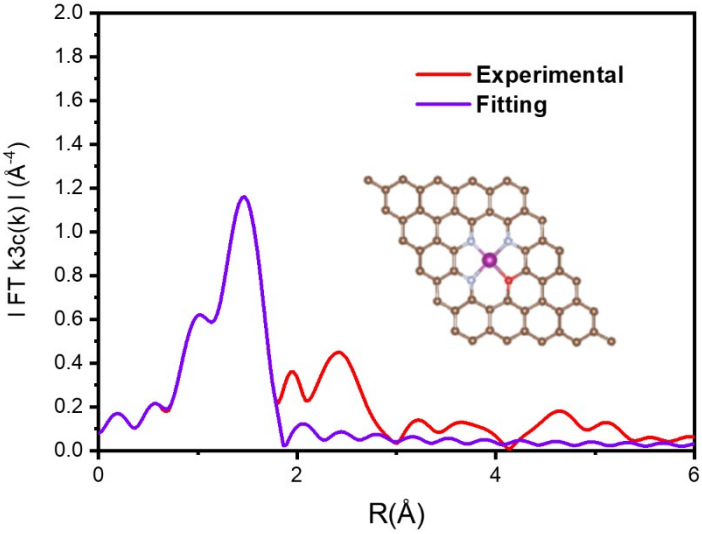

Figure S8. Fitting result of the FT EXAFS from Figure S7.

Table S2. Comparison of ORR activity of the as-prepared **Mn-N_x-NC** with the state-of-the-art catalysts in acidic and alkaline media, single-atom loading and atomic density of the previous reported literatures.

Sample	**Single atom**	**$E_{1/2}$ (V *vs.* RHE)**		**Loading content (%)**	**Ref.**
		Alkaline	**Acidic**		
Mn-SAs/NC	**Mn**	**0.91 (0.1 M KOH)**	**0.76 (0.5 M H_2SO_4)**	**0.67 at.%**	***This work***
Mn-N-C	Mn	--	0.80 (0.5 M H_2SO_4)	0.68 at.%	*Nat. Catal. 2018, 1, 935-945.*
Co_2/Fe–N@CHC	Co/Fe	0.915 (0.1 M KOH)	0.812 V (0.1 M $HClO_4$)	Co(0.41 at. %)/ Fe(0.19 at. %)	*Adv. Mater. 2021, 33, 2104718.*
Mn/C-NO	Mn	0.86	--	0.23 at.%	*Adv. Mater. 2018, 30, 1801732.*
Mn@NG	Mn	0.82	--	--	*Appl. Catal. B: Environ. 2019, 257, 117930.*
Fe-N_4 SAs/NC	Fe	0.885	--	1.96 at. %	*Angew. Chem. Int. Ed. 2018, 57, 8614.*
Fe SA-N-C	Fe	0.891	--	1.76 wt. %	*Angew. Chem. Int. Ed. 2018, 57, 8525.*
Co SAs/N-C	Co	0.881	--	4 wt. %	*Angew. Chem. Int. Ed. 2016, 55, 10800.*
Ni-MnO/rGO	Ni	0.78	--	--	*Adv. Mater. 2018, 30, 1704609.*
SA-Fe/NG	Fe	0.88	0.8 (0.1 M $HClO_4$)	--	*Proc. Natl. Acad. Sci. 2018, 115, 6626*
Fe/N-PCNs	Fe	0.86	--	--	*ACS. Appl. Mater. Interface 2020, 12,*

					13878.
FeCoNi/HCS	Fe/Co/Ni	0.85	--	--	*Nano Lett. 2021, 21, 3640−3648.*
ZnN_X/BP	Zn	0.85	0.66 (0.1 M $HClO_4$)	0.30 at.%	*Adv. Funct. Mater. 2017, 27, 1700802.*
ISAS Co/HNCS	Co	--	0.773 (0.5 M H_2SO_4)	2.2 wt. %	*J. Am. Chem. Soc. 2017, 139, 17269-17272.*
SA-Fe-HPC	Fe	0.89	0.81 (0.1 M H_2SO_4)	5.58 wt. %	*Angew. Chem. Int. Ed. 2018, 57, 9038-9043.*
Zn-N-C-1	Zn	0.873	0.746(0.1 M $HClO_4$)	5.64 wt. %	Angew. Chem. Int. Ed. 2019, 58, 7035.

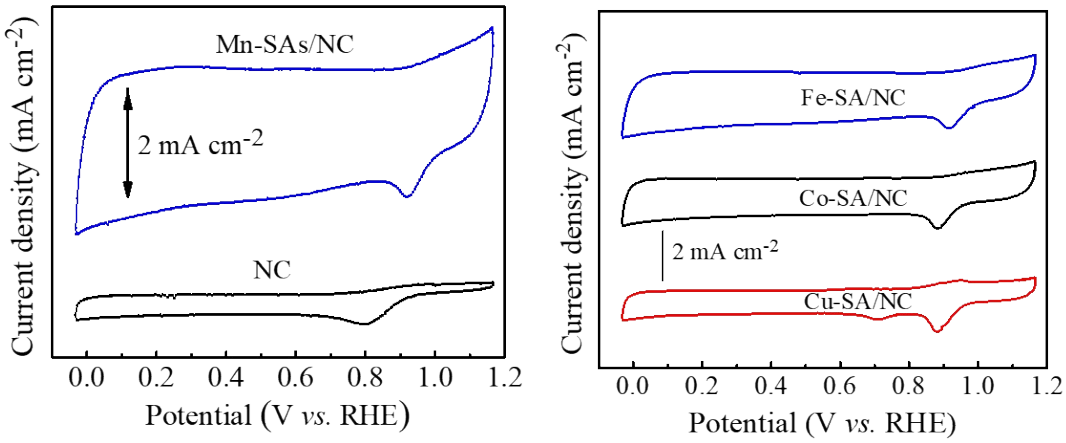

Figure S9. (a) CV curves of Mn-SAs/NC and NC samples obtained in O_2-saturated 1.0 M KOH electrolytes. (b) CV curves of other control samples including Fe-SAs/NC, Co-SAs/NC, and Cu-SAs/NC, obtained in O_2-saturated 1.0 M KOH electrolyte.

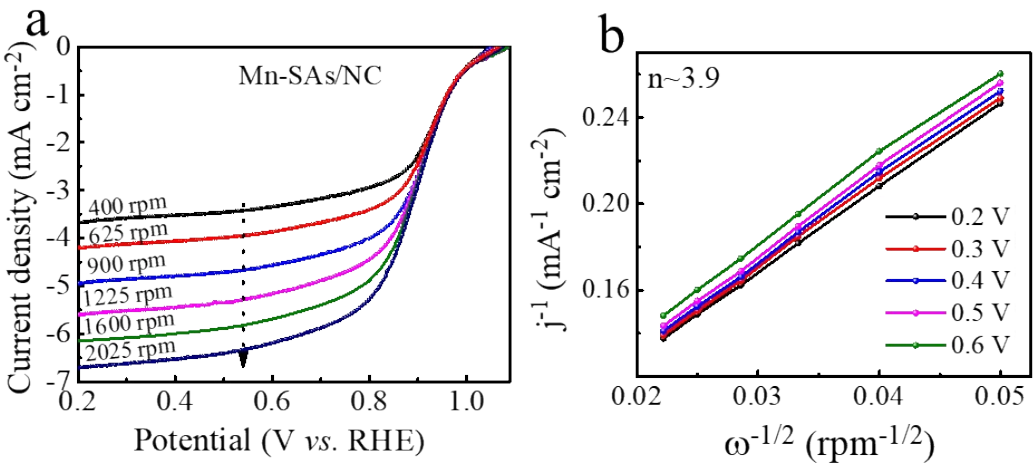

Figure S10. (a) ORR polarization curves of various Mn-SAs/NC samples in 0.1 M KOH at various rotating rates and (b) the corresponding K–L plots of Mn-SAs/NC

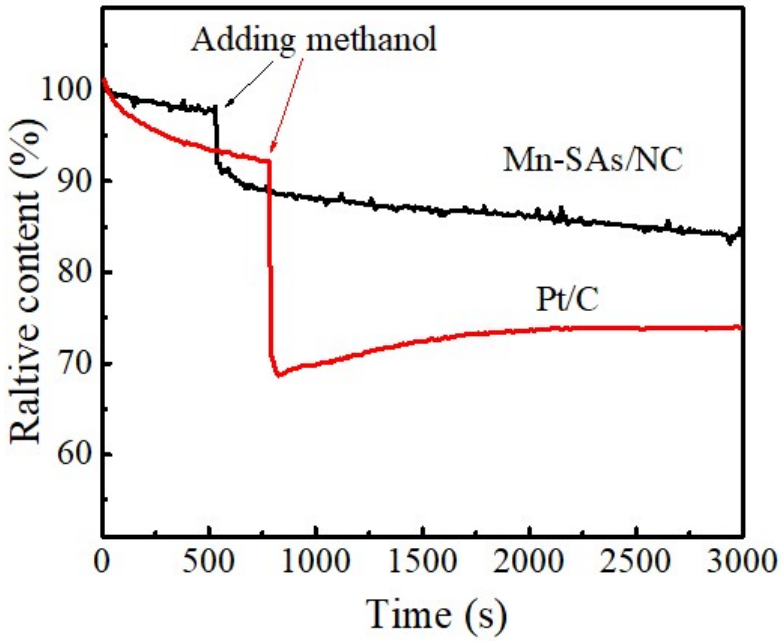

Figure S11. Chronoamperometric curves of as-prepared Mn-SAs/NC and Pt/C catalysts at 0.65 V (*vs.* RHE) in 0.1 M KOH solution with the addition of 20 mL methanol.

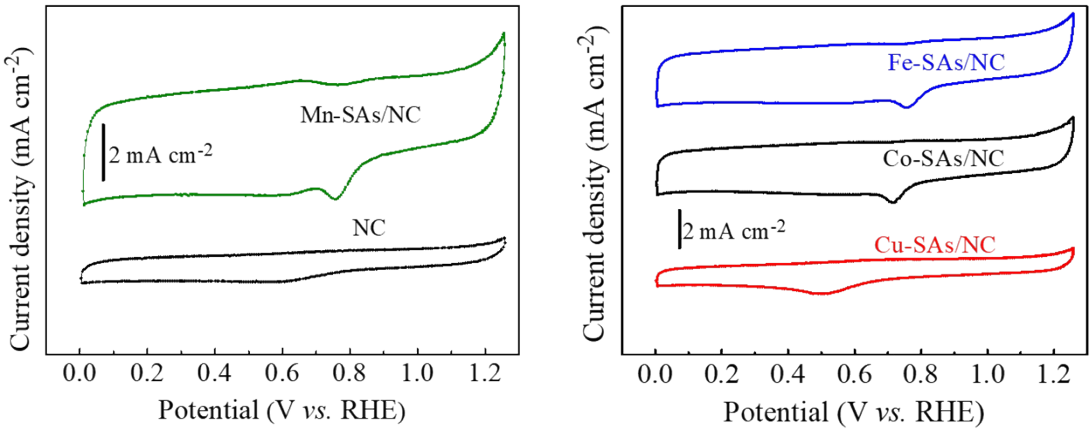

Figure S12. CV curves of NC, Mn-SAs/NC, and M (Fe, Co, and Cu)-SAs/NC catalysts obtained in N_2-saturated 0.5 M H_2SO_4 electrolytes.

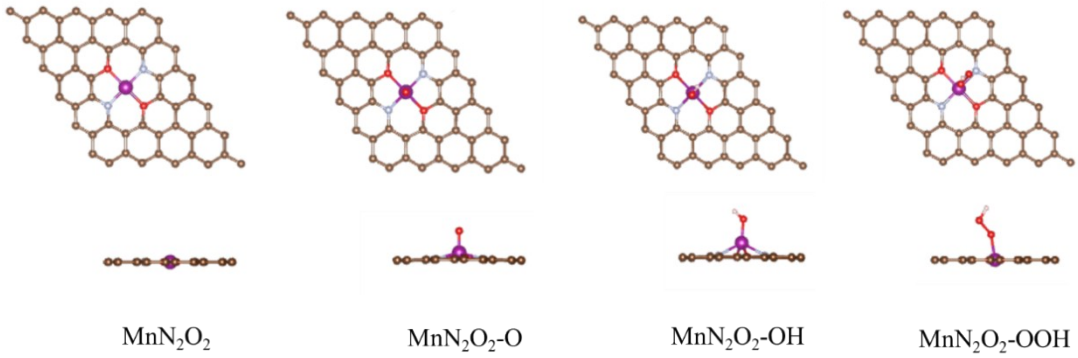

Figure S13. Top and side views of the optimized adsorption model of O*, OH*, and OOH* on MnN_2O_2 structure. Brown, purple, red, and white balls represent C, Mn, O, and N, respectively.

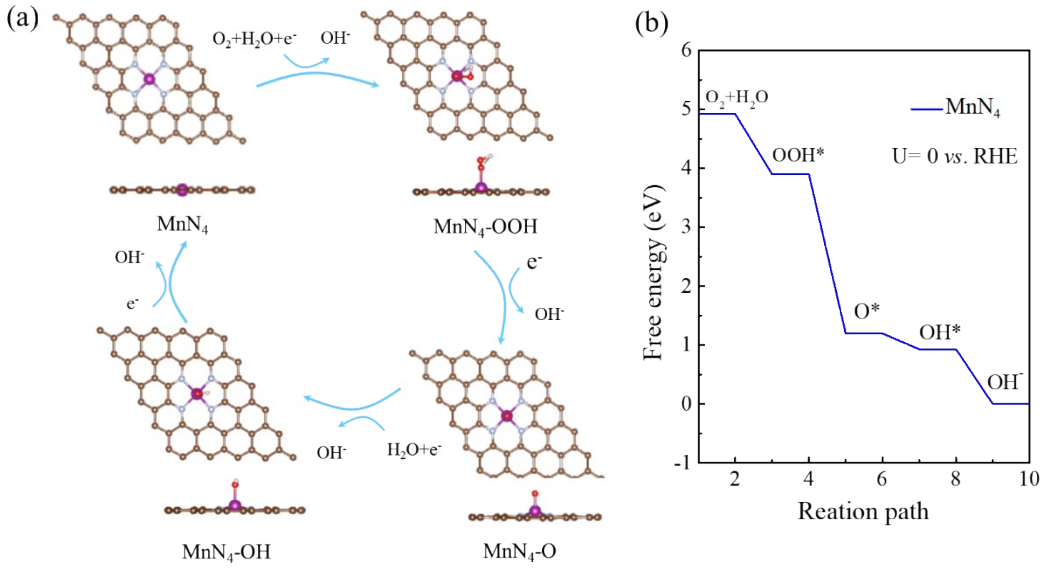

Figure S14. (a) Proposed ORR reaction scheme of MnN_4 model with optimized geometry and the intermediates in alkaline media. (C: brown, Mn: purple, O: red, and N: white balls.) (b) Free energy diagram for ORR of MnN_4 model at 0 V.

1. Gan, G.; Li, X.; Wang, L.; Fan, S.; Mu, J.; Wang, P.; Chen, G., Active Sites in Single-Atom Fe–N_x–C Nanosheets for Selective Electrochemical Dechlorination of 1,2-Dichloroethane to Ethylene. *ACS Nano* **2020,** *14* (8), 9929-9937.

2. Zhou, Y.; Tao, X.; Chen, G.; Lu, R.; Wang, D.; Chen, M.-X.; Jin, E.; Yang, J.; Liang, H.-W.; Zhao, Y.; Feng, X.; Narita, A.; Müllen, K., Multilayer stabilization for fabricating high-loading single-atom catalysts. *Nature Communications* **2020,** *11* (1), 5892.

3. Li, M.; Wu, S.; Yang, X.; Hu, J.; Peng, L.; Bai, L.; Huo, Q.; Guan, J., Highly efficient single atom cobalt catalyst for selective oxidation of alcohols. *Applied Catalysis A: General* **2017,** *543*, 61-66.

4. Chen, K.; Kim, S.; Je, M.; Choi, H.; Shi, Z.; Vladimir, N.; Kim, K. H.; Li, O. L., Ultrasonic Plasma Engineering Toward Facile Synthesis of Single-Atom M-N_4/N-Doped Carbon (M = Fe, Co) as Superior Oxygen Electrocatalyst in Rechargeable Zinc–Air Batteries. *Nano-Micro Letters* **2021,** *13* (1), 60.

5. Tong, M.; Sun, F.; Xie, Y.; Wang, Y.; Yang, Y.; Tian, C.; Wang, L.; Fu, H., Operando Cooperated Catalytic Mechanism of Atomically Dispersed Cu−N4 and Zn−N_4 for Promoting Oxygen Reduction Reaction. *Angewandte Chemie International Edition* **2021,** *60* (25), 14005-14012.

6. Chen, T.; Zhu, Z.; Zhang, H.; Qiu, Y.; Yin, D.; Zhao, G., Facile Construction of a Copper-Containing Covalent Bond for Peroxymonosulfate Activation: Efficient Redox Behavior of Copper Species via Electron Transfer Regulation. *ACS Applied Materials & Interfaces* **2020,** *12* (38), 42790-42802.

7. Liu, M.; Lee, J.; Yang, T.-C.; Zheng, F.; Zhao, J.; Yang, C.-M.; Lee, L. Y. S., Synergies of Fe Single Atoms and Clusters on N-Doped Carbon Electrocatalyst for pH-Universal Oxygen Reduction. *Small Methods* **2021,** *5* (5), 2001165.

8. Zhu, C.; Shi, Q.; Xu, B. Z.; Fu, S.; Wan, G.; Yang, C.; Yao, S.; Song, J.; Zhou, H.; Du, D.; Beckman, S. P.; Su, D.; Lin, Y., Hierarchically Porous M–N–C (M = Co and Fe) Single-Atom Electrocatalysts with Robust MNx Active Moieties Enable Enhanced ORR Performance. *Advanced Energy Materials* **2018,** *8* (29), 1801956.

9. Fu, Y.; Wei, Q.; Zhang, G.; Wang, X.; Zhang, J.; Hu, Y.; Wang, D.; Zuin, L.; Zhou, T.; Wu, Y.; Sun, S., High-Performance Reversible Aqueous Zn-Ion Battery Based on Porous MnOx Nanorods Coated by MOF-Derived N-Doped Carbon. *Advanced Energy Materials* **2018,** *8* (26), 1801445.